Mechanisms of Hf Dopant Incorporation during the Early Stage of Chemical Vapor Deposition Aluminide Coating Growth under Continuous Doping Conditions

G.Y. KIM, L.M. HE, J.D. MEYER, A. QUINTERO, J.A. HAYNES, and W.Y. LEE

A laboratory-scale chemical vapor deposition (CVD) reactor was used to perform "continuous" Hf doping experiments while the surface of a single-crystal Ni alloy was being aluminized to form an aluminide (β-NiAl) coating matrix for 45 minutes at 1150 °C. The continuous doping procedure, in which $HfCl_4$ and $AlCl_3$ were simultaneously introduced with H_2, required a high $HfCl_4/AlCl_3$ ratio ($>\sim 0.6$) to cause the precipitation of Hf-rich particles (~ 0.1 μm) at grain boundaries of the coating layer, with the overall Hf concentration of ~ 0.05 to 0.25 wt pct measured in the coating layer by glow-discharge mass spectroscopy (GDMS). Below this ratio, Hf did not incorporate as a dopant into the growing coating layer from the gas phase, as the coating matrix appeared to be "saturated" with other refractory elements partitioned from the alloy substrate. In comparison, the Hf concentration in the aluminide coating layer formed on pure Ni was in the range of ~ 0.1 wt pct, which was close to the solubility of Hf estimated for bulk NiAl. Interestingly, the segregation of Hf and the formation of a thin γ'-Ni_3Al layer (~ 0.5 μm) at the coating surface were consistently observed for both the alloy and pure-Ni substrates. The formation of the thin γ'-Ni_3Al layer was attributed to an increase in the elastic strain of the β-NiAl phase, associated with the segregation of Hf as well as other refractory alloying elements at the coating surface. This phenomenon also implied that the coating layer was actually growing at the interface between the γ'-Ni_3Al layer and the β-NiAl coating matrix, not at the gas/coating interface, during the early stage of the coating growth.

I. INTRODUCTION

DIFFUSION aluminide coatings produced by pack cementation, gas-phase pack, and chemical vapor deposition (CVD) have been successfully developed and used over the past 50 years to protect Ni alloy components from high-temperature environments encountered in aircraft engines and land-based gas turbines.[1] Recently, aluminide coatings have been adapted for use as bond coatings for thermal barrier coatings (TBCs).[2] State-of-the-art TBCs consist of a strain-tolerant, thermally insulating, Y_2O_3-stabilized ZrO_2 (YSZ) layer prepared by electron beam physical vapor deposition (EBPVD). A bond coating protects the underlying alloy from oxidation by forming an adherent thermally grown oxide (TGO) at the bond coating / YSZ interface. The dominant failure mode observed in EBPVD TBCs is progressive TGO damage and consequent TBC delamination upon oxidation and repeated thermal cycling.[3,4,5] Therefore, improving the scale-adhesion behavior of bond coatings is a critical issue in the development of more reliable TBCs.

One potent way of improving the quality of a TGO, and, therefore, its adhesion, is to dope Ni-based alloys with a small amount of "reactive elements" such as Y, Hf, Zr, *etc.*[6,7,8] Recent experimental observations with model bond-coating materials have shown that the cyclic oxidation life of an EBPVD-TBC layer significantly improves when cast NiAl doped with Zr or Hf is used as a substrate.[9] The beneficial effects of reactive elements in Ni and coating alloys have been extensively studied and discussed thoroughly.[6,10–13] Some coating work has been conducted to incorporate Y, Zr, and/or Hf during aluminizing by pack cementation or gas-phase pack.[11,14] Also, other hybrid methods have been pursued.[15,16] However, in actual manufacturing practice, these coating approaches are found to be unsuitable[17] because of inherent processing irreproducibility in terms of precisely controlling the dopant concentration and distribution in the coating matrix. Prior studies with bulk alloys and intermetallics have certainly shown that, in order for its beneficial effect to be operative, a reactive element must be present at a well controlled characteristic level and distribution in the matrix materials.[7,18,19]

Recent manufacturing advances in aluminizing by CVD offer new processing opportunities to significantly improve the performance of single-phase β-NiAl and (Ni,Pt)Al bond coatings for next-generation TBC applications.[20,21] As has been previously elaborated,[22] the dynamic versatility of the CVD aluminizing process provides an avenue for uniformly doping the coating matrix with a reactive element (*e.g.*, Hf) *via* proactive control of the gas-phase concentration of its precursor ($HfCl_4$) as a function of time. However, with the apparent lack of meaningful experimental results, considerable uncertainties exist to properly project the viability of the doping approach for proactively controlling the dopant concentration and distribution. The goal of this study was to examine the incorporation behavior of Hf into the coating matrix during the early stages of aluminizing the surface of a single-crystal Ni superalloy under continuous doping conditions.

G.Y. KIM, Senior Process Design Engineer, Process Technology Group, is with Genus, Inc., Sunnyvale, CA. L.M. HE, Postdoctoral Researcher, is with the Chemical Engineering Department, Georgia Institute of Technology, Atlanta, GA. J.D. MEYER, Ph.D. Candidate, and W.Y. LEE, Professor, are with the Chemical, Biomedical, and Materials Engineering Department, Stevens Institute of Technology, Hoboken, NJ. Contact e-mail: wlee@stevens.edu. A. QUINTERO, Associate Professor, is with the Universidad Central de Venezuela, Caracas, Venezuela. J.A. HAYNES, Staff Member, is with the Oak Ridge National Laboratory, Oak Ridge, TN.

Manuscript submitted January 22, 2001.

II. EXPERIMENTAL

A. *Preparation of Substrates*

A single-crystal Ni alloy (RENÉ* N5) was cast as a cylindrical rod with a [100] seed direction. The alloy rod was sliced radially to produce disc specimens (0.2 cm in thickness × 1.2 cm in diameter) while preserving the [100] orientation on the disc surface. The nominal composition (in wt pct) of the alloy is 6.2Al, 0.05C, 7.5Co, 7.0Cr, 0.16Hf, 1.5Mo, 3.0Re, 6.5Ta, 0.02Ti, 5.0W, and Ni as the balance. The specimen surface was polished using a procedure described elsewhere.[21] Notice that the Ni alloy substrate contains Hf and other refractory alloying elements like Ta and W, which incorporate into the coating layer during aluminide coating formation, as will be discussed in the Results Section. In order to study the Hf incorporation behavior in the aluminide coating in the absence of the other alloying elements, a long polycrystalline Ni (99.99 pct purity) strip (10 × 1 × 0.5 cm) was also used as a model substrate.

*RENÉ is a trademark of General Electric Company, Fairfield, CT.

B. *The CVD Reactor*

As schematically shown in Figure 1, a hot-wall CVD reactor interfaced with a sample loading chamber was used to conduct a series of Hf doping experiments. A reactor chamber and a sample holder were made of IN600 and prealuminized by pack cementation prior to the present study. A stainless steel sample loading chamber, along with a magnetic transporter, was used for rapid insertion and retrieval of the substrate holder from the hot reactor chamber. The ability to rapidly quench the aluminized coating doped with Hf was important to minimize Hf diffusion, which might occur during slow furnace cooling. It was estimated by heat-conduction calculations that the surface temperature of the substrates could be cooled to ~200 °C in a few minutes during the retrieval of the sample holder from the reactor chamber to the sample loading chamber.

$AlCl_3$ and $HfCl_4$ were generated by chlorinating metallic Al (99.99 pct) and Hf (99.95 pct) pellets with HCl (99.999 pct) at ~300 °C and ~400 °C, respectively, using stainless steel chlorinators, as shown in Figure 1. For some preliminary experiments, a diluted HCl gas (0.5 pct HCl in Ar) was used to produce a low flow rate of $HfCl_4$. The gas lines from the chlorinators to the reactor were heated to ~400 °C to avoid the condensation of $HfCl_4$ and $AlCl_3$, since $HfCl_4$ sublimes at 316 °C and $AlCl_3$ sublimes at 178 °C. The flow rates of HCl, H_2 (99.999 pct), and Ar (99.999 pct) were controlled by mass-flow meters.

C. *Continuous Doping Procedure*

Continuous doping experiments included three consecutive steps: (1) 20 minutes of aluminizing with $AlCl_3$ and H_2 at 1150 °C and 13 kPa, (2) 15 minutes of simultaneously feeding $HfCl_4$ as the gaseous dopant precursor with the $AlCl_3 + H_2$ mixture, and (3) 10 minutes of aluminizing with the $AlCl_3 + H_2$ mixture, as schematically shown in Figure 2. The processing conditions used for the experiments are listed in Table I.

The first step of "pure" aluminizing was introduced to establish the columnar microstructure of the aluminide coating layer. (Our earlier study[23] showed that it takes about 20 minutes of aluminizing for the growth of a fully developed columnar β-NiAl coating matrix.) The pure aluminizing procedure was as follows. The reactor chamber was heated to 1150 °C (±5 °C) in flowing H_2. Prior to inserting the sample holder into the hot reactor chamber, both the reactor and sample loading chambers were evacuated to ~13 Pa. After the substrate holder was inserted into the reactor chamber, the reactor pressure was increased to 13.3 kPa using H_2, and $AlCl_3$ was then fed into the reactor to start the aluminizing step. The flow rate of H_2 was 300 cm^3/min at standard temperature and

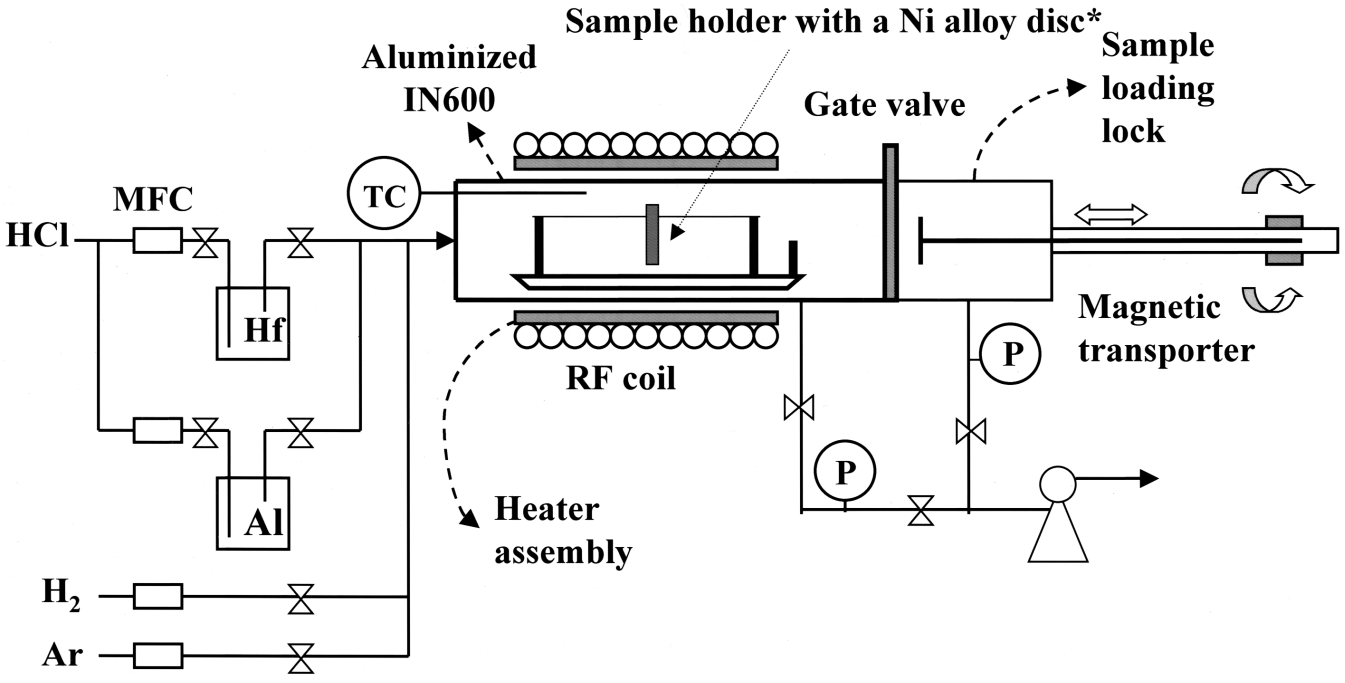

Fig. 1—Schematic Diagram of the Laboratory Scale CVD Reactor Used for Hf Doping Experiments.

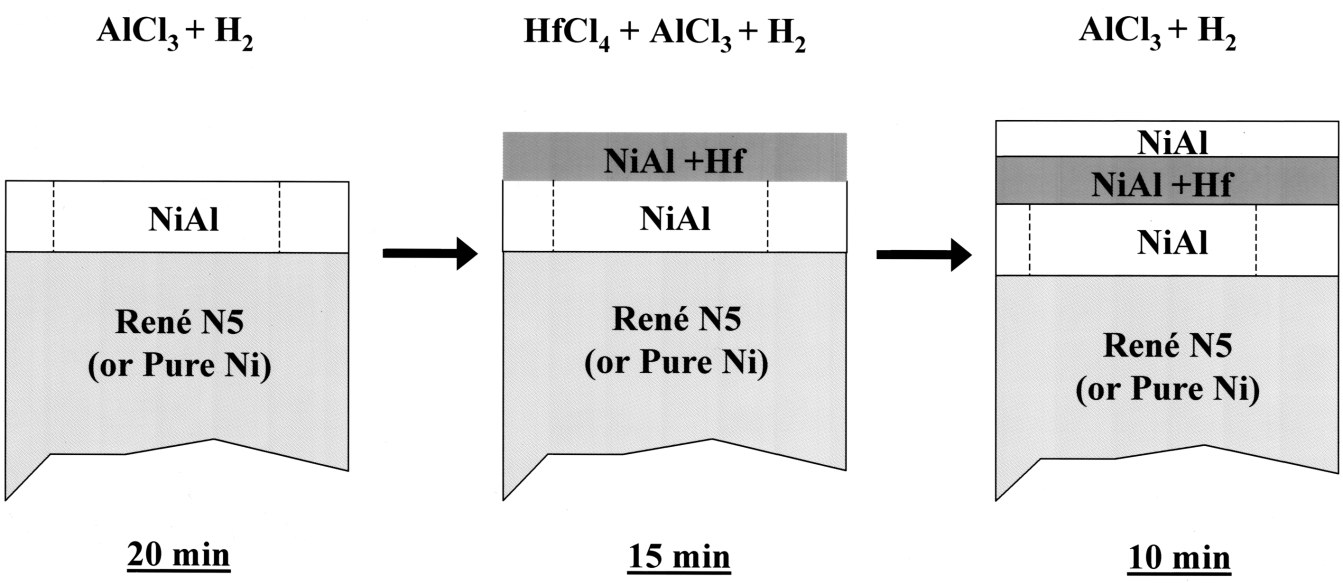

Fig. 2—Schematic illustration of the continuous doping procedure.

Table I. Processing Conditions Used for the Continuous Hf Doping Experiments Performed with Ni Superalloy Substrate

Partial Pressure Ratio	Sequence	Gas Flow Rate (cm^3/min at STP)					T (°C)	P (kPa)
		HCl for Al	HCl for Hf	H_2	Ar	Total		
$P_{HfCl_4}/P_{AlCl_3} = 0.02$	step 1 (20 min)	50	0	300	0	350	1150	13.3
	step 2 (15 min)	50	2	300	38	390	1150	13.3
	step 3 (10 min)	50	0	300	0	350	1150	13.3
$P_{HfCl_4}/P_{AlCl_3} = 0.13$	step 1 (20 min)	50	0	300	0	350	1150	13.3
	step 2 (15 min)	50	10	300	200	560	1150	13.3
	step 3 (10 min)	50	0	300	0	350	1150	13.3
$P_{HfCl_4}/P_{AlCl_3} = 0.6$	step 1 (20 min)	50	0	300	0	350	1150	13.3
	step 2 (15 min)	50	50	300	0	400	1150	13.3
	step 3 (10 min)	50	0	300	0	350	1150	13.3
$P_{HfCl_4}/P_{AlCl_3} = 0.67$	step 1 (20 min)	50	0	300	0	350	1150	13.3
	step 2 (15 min)	50	50	300	200	600	1150	13.3
	step 3 (10 min)	50	0	300	0	350	1150	13.3

pressure, while that of the HCl flow used to chlorinate Al pellets was 50 cm^3/min (*i.e.*, $AlCl_3$ flow rate = 16.7 cm^3/min).

For the second step, $HfCl_4$ was introduced while the $AlCl_3 + H_2$ mixture was continually fed into the reactor for 15 minutes (*i.e.*, "continuous" doping). During this sequence, the inlet $HfCl_4$ concentration in the gas phase of the CVD reactor could be systematically varied by changing the HCl flow rate through the Hf chlorinator while keeping that of $AlCl_3$ constant at 16.7 cm^3/min, as listed in Table I. In order to start the third step of the continuous doping procedure, the $HfCl_4$ flow was stopped while the $AlCl_3$ and H_2 flows continued for another 10 minutes (*i.e.*, back to pure aluminizing). The third step was added to assess the relative mobility of Hf after its incorporation into the coating matrix during the second step. At the end of the third step, the $AlCl_3$ and H_2 flows were stopped, the reactor chamber was evacuated, and the substrate holder was retrieved from the hot reactor chamber to the sample loading chamber.

Similar continuous doping experiments were also performed using pure-Ni substrates, as summarized in Table II. Since the size of the pure-Ni substrate was substantially larger (10 × 1 × 0.5 cm), the HCl flow rate used to chlorinate Al was higher in order to minimize the depletion of $AlCl_3$ along the flow direction of the reactor chamber. Also, higher $HfCl_4/AlCl_3$ partial-pressure ratios were used than those for the Ni alloy specimens, based on initial characterization results obtained for the alloy specimens.

D. *Characterization*

A scanning electron microscope (SEM), equipped with a field-emission gun and an energy-dispersive spectrometer (EDS), was used for microstructure characterization and qualitative compositional evaluation. Some coating samples were cross sectioned metallographically, and an etchant ($5HCl \cdot 1HNO_3$) was used to highlight phase contrast. An X-ray diffractometer (XRD) with grazing-incidence-detector scan capabilities was used for phase determination. A transmission electron microscope (TEM) was also used to confirm the presence and the location of the major phases observed by XRD in some of the coating specimens. For TEM specimen preparation, coated specimens of interest were placed between two single-crystal Si wafer pieces using an epoxy adhesive. The "sandwich" specimens were then cured

Table II. Processing Conditions Used for the Continuous Hf Doping Experiments Performed with Pure Ni Substrate

Partial Pressure Ratio	Sequence	Gas Flow Rate (cm^3/min at STP)					T (°C)	P (kPa)
		HCl for Al	HCl for Hf	H_2*	Ar**	Total		
$P_{HfCl_4}/P_{AlCl_3} = 0.19$	step 1 (20 min)	100	0	200	750	1050	1150	13.3
	step 2 (15 min)	100	25	250	675	1050	1150	13.3
	step 3 (10 min)	100	0	200	750	1050	1150	13.3
$P_{HfCl_4}/P_{AlCl_3} = 0.75$	step 1 (20 min)	100	0	200	750	1050	1150	13.3
	step 2 (15 min)	100	100	400	450	1050	1150	13.3
	step 3 (10 min)	100	0	200	750	1050	1150	13.3
$P_{HfCl_4}/P_{AlCl_3} = 1.87$	step 1 (20 min)	100	0	200	750	1050	1150	13.3
	step 2 (15 min)	100	250	700	0	1050	1150	13.3
	step 3 (10 min)	100	0	200	750	1050	1150	13.3

*The flow rate of H_2 was varied to keep the constant ratio of $(AlCl_3 + HfCl_4)/H_2$ during step 2 of the continuous doping procedure.
**The flow rate of Ar was varied to keep the total flow rate constant at 1050 cm^3/min.

for 2 hours at 170 °C in air, were cross sectioned to small coupons of 0.5 × 2 × 5 mm, and were thinned by the tripod polishing method.[24]

The elemental composition of coating specimens was analyzed as a function of coating depth by glow-discharge mass spectroscopy (GDMS). This technique utilizes a glow-discharge plasma ball (~1 to 2 cm in diameter) to sputter a solid surface under high vacuum. Meanwhile, a high-resolution mass spectrometer equipped with a double-focusing sector is used to detect elements being sputtered away from the solid surface. This technique was used because of its ability to detect major, minor, trace, and ultratrace elements (*i.e.*, parts per million to percent) in the same analytical cycle.[25,26] The GDMS technique was developed mainly for trace-element analysis of bulk specimens; therefore, the application of this technique to our thick-coating specimens should be approached cautiously for several reasons. From prior work,[21] it was found that GDMS analysis could not be used for quantitative depth profiling, due to the formation of a highly nonuniform crater on the coating surface. Nevertheless, the compositional profiles of major elements such as Ni, Al, Cr, and Co measured by GDMS were in agreement with electron microprobe data. More importantly, the technique was useful for locating the parts per million level of sulfur segregation at the coating surface and the coating/substrate interface regions.

Based on the prior experience, the GDMS technique was mainly used in this study to detect Hf below the resolution limit of an electron microprobe (~0.1 to 0.2 wt pct). Also, some coating specimens were analyzed by electron microprobe analysis (EMPA) with a spot size of ~0.5 μm, for comparison to the GDMS results. For the coatings formed on the Ni alloy, the nominal Hf composition in this alloy (0.16 wt pct) was used as an internal standard to calibrate the GDMS instrument. For the coatings formed on the pure-Ni substrate, a cast NiAl specimen with 0.04 at. pct Hf, as previously measured at Oak Ridge National Laboratory, was used to calibrate the instrument.

III. RESULTS

A. *Continuous Hf Doping Experiments with Ni Alloy Substrate*

Coating specimens produced by the continuous doping procedure at the $HfCl_4/AlCl_3$ ratios of 0.13 and 0.60 are shown in Figures 3(b) and (c). The microstructure of the coating specimens was similar to that of the coating formed without Hf doping (*i.e.*, $HfCl_4/AlCl_3$ ratio = 0), as shown in Figure 3(a) for comparison. As previously described in our earlier study,[23] the "low-activity" aluminide coating produced by CVD consisted of three distinct layers: a thin layer of γ'-Ni_3Al at the coating surface, an external β-NiAl coating layer, and a diffusion zone between the coating layer and the Ni-alloy substrate.

In the external coating layer, the grain boundaries originated at the substrate surface and extended to the coating surface. The grain boundaries were decorated with a linear array of very fine bright-contrast particles.[23] For example, Figure 3 shows that the presence of bright-contrast particles increased with increasing $HfCl_4/AlCl_3$ ratio. The composition of these particles could not be determined by EMPA because of the spatial and composition resolution limitations (~0.1 μm and ~0.1 wt pct, respectively) of the EMPA technique. The coating thickness was not strongly influenced by the changes in the $HfCl_4/AlCl_3$ partial-pressure ratio (Figures 3(b) and (c)). However, the thickness of the Hf-doped aluminide layer formed was thinner (~1.8 μm) than that of the pure aluminide coating formed for the same aluminizing time (45 minutes), as shown in Figure 3.

Underneath the coating layer, a diffusion zone with precipitates enriched with alloying elements (which appear as bright-contrast particles in the micrographs in Figure 3) was formed due to the outward diffusion of Ni from the alloy to form the external aluminide coating layer. It was previously explained[27] that the loss of Ni in the alloy surface region results in the transformation of the original γ/γ' structure to the β-NiAl phase, with the precipitates enriched with refractory elements due to their lower solubility in the β-NiAl phase.

In Figure 4, the XRD patterns of the aluminide-coating specimens without Hf doping (Figure 4(a)) and of those doped at the $HfCl_4/AlCl_3$ ratio of 0.67 (Figure 4(b)) are compared. The aluminide coating matrix formed without Hf doping showed a strong preferred orientation of β-NiAl grains to the [110] orientation with a very weak peak of (111) γ'-Ni_3Al, as evident from the normal θ-2θ scan (Figure 4(a)). However, the grazing-incidence XRD pattern in Figure 4(a) suggested that the phase of the coating surface was different from that of the coating matrix, as the (111) γ'-Ni_3Al peak became stronger.

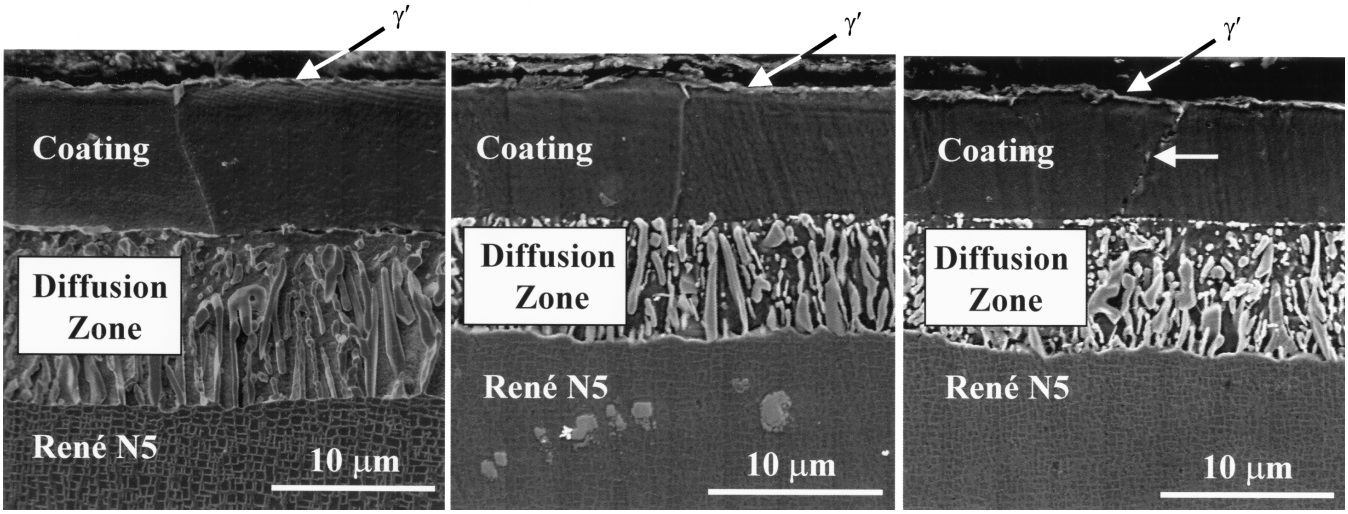

Fig. 3—SEM cross-section images of the aluminide coating specimens formed on the Ni alloy at the $HfCl_4/AlCl_3$ partial pressure ratio of (*a*) 0, (*b*) 0.13, and (*c*) 0.6.

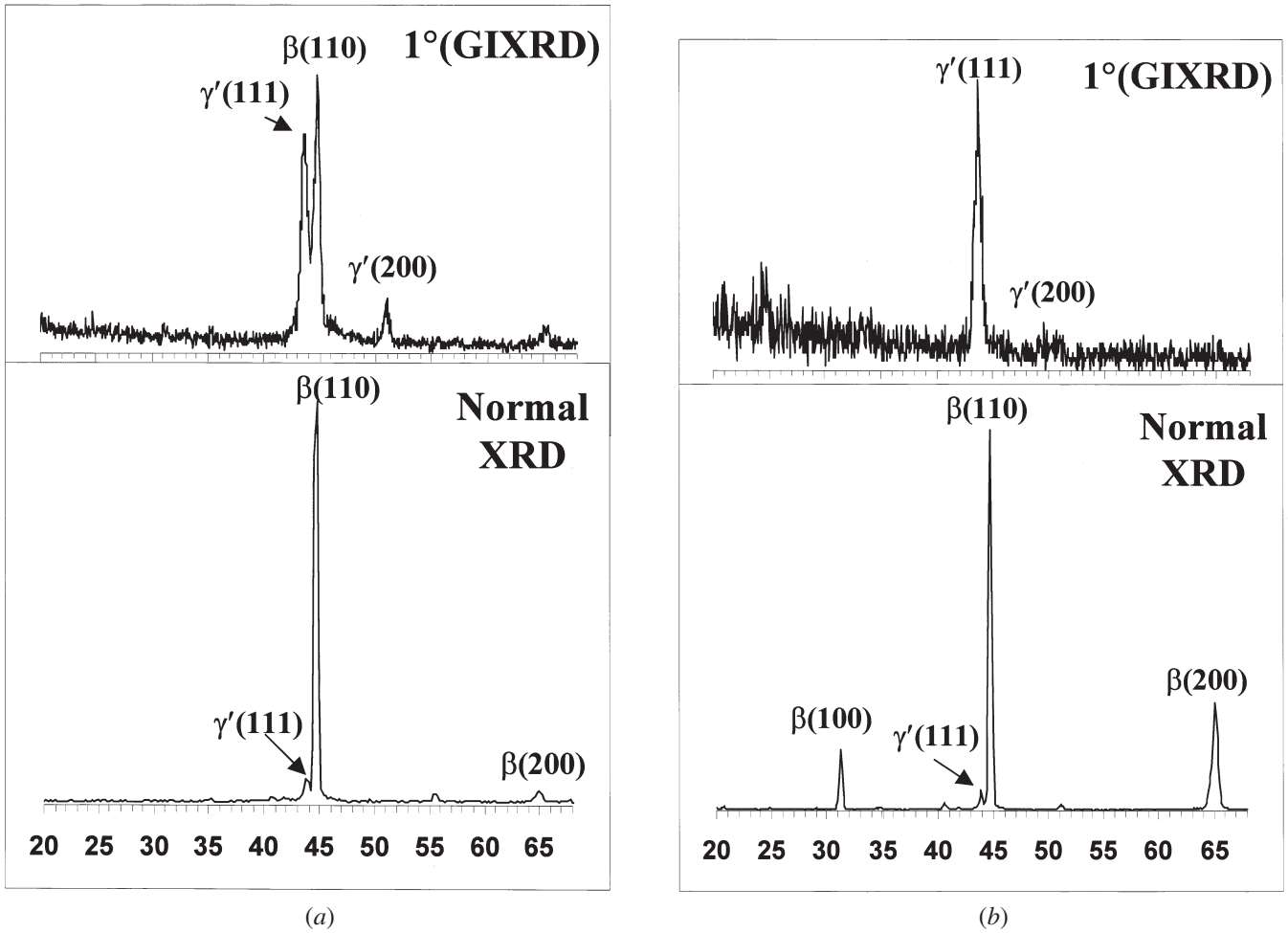

Fig. 4—XRD patterns of the aluminide coating specimens formed on the Ni alloy at the $HfCl_4/AlCl_3$ ratio of (*a*) 0 and (*b*) 0.67.

In comparison, the coating matrix doped with Hf was less preferentially oriented, as the relative dominance of the $\beta(110)$ peak decreased with the appearance of the $\beta(100)$ and $\beta(200)$ peaks in the normal θ-2θ scan in Figure 4(b). The grazing-incidence XRD pattern in Figure 4(b) showed a strong peak from the (111) plane of γ'-Ni_3Al and the

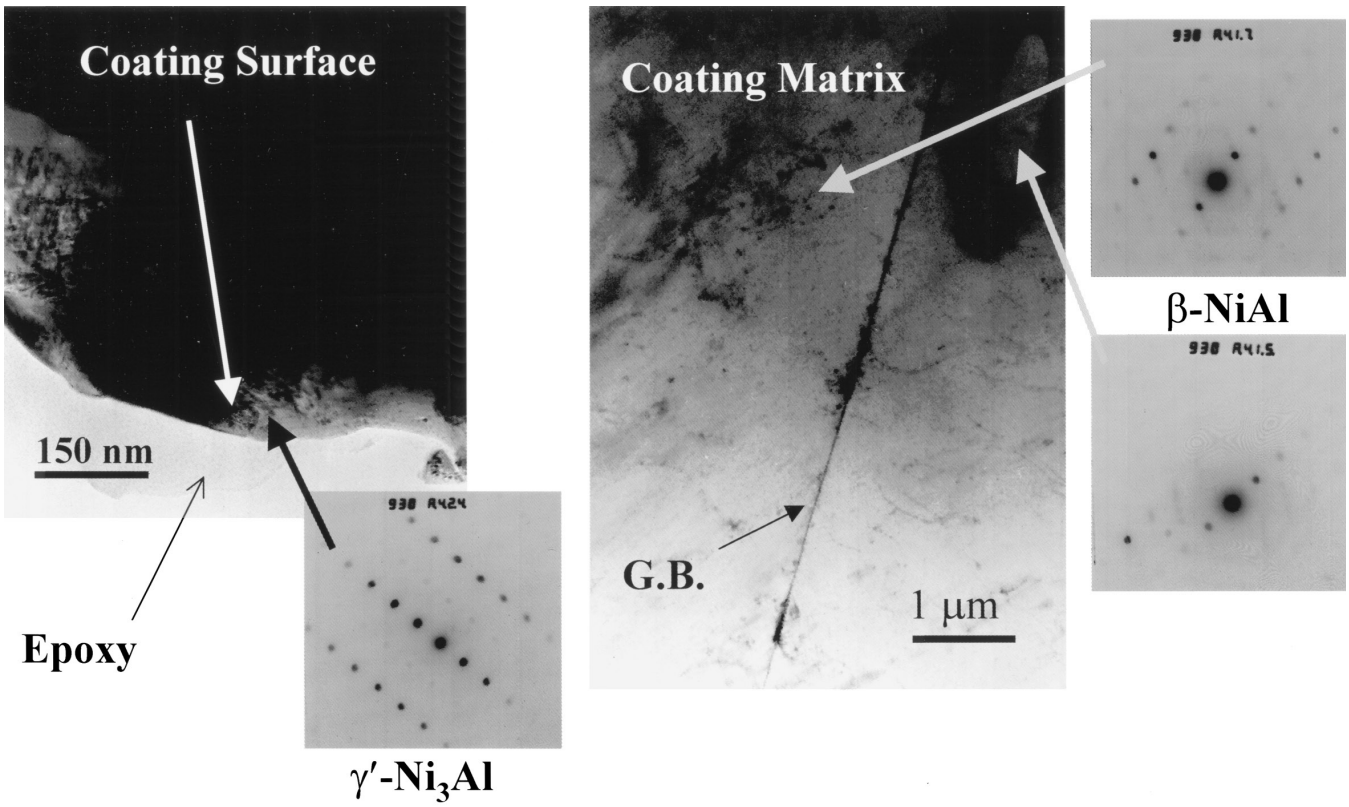

Fig. 5—TEM images and diffraction patterns of the aluminide coating formed on Ni alloy at the $HfCl_4/AlCl_3$ ratio of 0.67.

disappearance of the $\beta(110)$ peak at the coating surface. The TEM results in Figure 5 show that a thin layer of γ'-Ni_3Al ($\sim$0.5 μm) was present at the coating surface. Electron diffraction patterns obtained at the coating-surface region were indexed to γ'-Ni_3Al, whereas the coating matrix was confirmed to be β-NiAl by electron diffraction.

The depth profiles of Hf were analyzed as a function of the $HfCl_4/AlCl_3$ ratio by GDMS, as shown in Figure 6(a). The profiles were normalized based on the average depth of sputtered craters measured by metallography and SEM, as well as the nominal Hf concentration in the Ni-alloy substrate. Three distinctive regions (*i.e.*, the coating layer, the diffusion zone, and the substrate) were observed with increasing sputtering time. Note that the GDMS composition data at the very top surface of these coating specimens were not obtained (as marked in Figure 6), because it took about $\sim$5 minutes to stabilize the DC discharge for these samples. Since the sputtering rate was $\sim$0.2 μm/min, $\sim$1 μm of the coating surface was removed before the first Hf composition data could be collected.

At low-Hf doping conditions, no significant increase of Hf concentration was observed in the coating layer with an increasing $HfCl_4/AlCl_3$ partial-pressure ratio from 0.02 to 0.13. The Hf concentration in the coating layer was very low ($\sim$0.01 wt pct) at these ratios. In Figure 7, the Hf and Ta profiles of the coating produced at the $HfCl_4/AlCl_3$ partial-pressure ratio of 0.13 are compared. Note that the Ni alloy used in this study nominally contains $\sim$0.16 wt pct Hf and $\sim$6.5 wt pct Ta. The Ta concentrations measured in the coating layer and the substrate by GDMS were $\sim$0.9 and $\sim$5.7 wt pct, respectively. The low concentrations of Hf and Ta in the coating layer and their similar profiles suggested that the coating layer was "autodoped" with the Hf and Ta originally existing in the alloy substrate during coating growth.

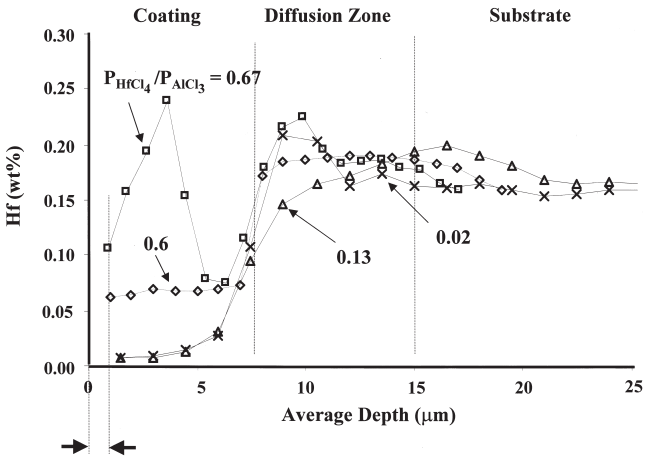

Fig. 6—GDMS compositional profiles of Hf through the aluminide coating formed on the Ni alloy at the $HfCl_4/AlCl_3$ ratio of 0.02, 0.13, 0.60, and 0.67.

It is important to point out that the Gaussian-looking slope of the Hf profiles at the coating/diffusion-zone interface region (Figures 6 and 7) was caused by the formation of nonuniform craters during sputtering.[21] In this regard, the slope did not necessarily represent the presence of a continuous concentration gradient, due to the slow diffusion of Hf into the coating layer. The Hf and Ta concentration changes at the interface should be interpreted as being "partitioned"

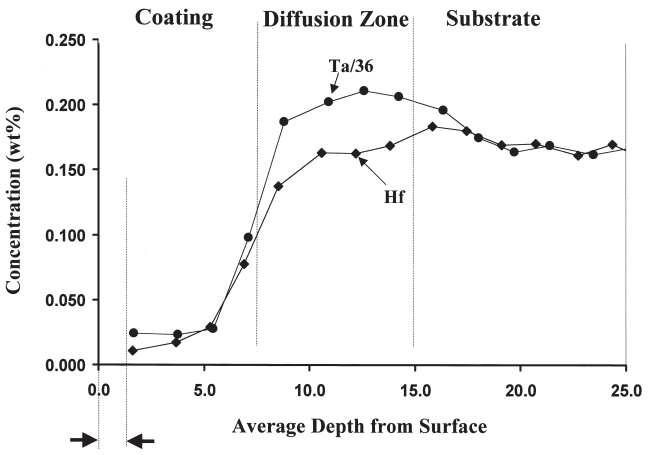

Fig. 7—Comparison of Hf and Ta GDMS profiles of the aluminide coating formed on the Ni alloy at the $HfCl_4/AlCl_3$ ratio of 0.13.

instead of "diffused." The SEM and EDS analysis also suggested that compositional changes for all alloying elements were sharp at the interface between the coating layer and the diffusion zone.

In the diffusion zone (Figure 6), the Hf profiles showed a weak relationship to the doping conditions, but showed evidence for some segregation at the coating/diffusion-zone interface. As shown in Figure 3, refractory alloying elements like Ta and Hf from the Ni alloy segregated to form the precipitates, as the γ/γ' alloy structure was changed to the β-NiAl phase. These Hf profiles became uniform at the nominal Ni-alloy Hf level as sputtering penetrated deep into the alloy substrate and under the diffusion zone. By increasing the $HfCl_4/AlCl_3$ ratio to 0.6 (Figure 6(a)), the Hf concentration in the coating layer formed on the Ni alloy increased to ~0.06 wt pct with a relatively constant profile through the coating thickness. As the $HfCl_4/AlCl_3$ ratio increased to 0.67, the peak Hf concentration of ~0.25 wt pct was measured at the middle of the coating layer. Even at the highest $HfCl_4/AlCl_3$ ratio of 0.67 in the gas phase, the Hf/Al atomic ratio in the coating layer was measured to be only ~0.005. The implications of this low-Hf-incorporation behavior will be discussed later.

B. *Continuous Hf Doping Experiments with Pure Ni*

All aluminide coating specimens produced on pure Ni substrates by the continuous doping procedure retained their columnar microstructure. As shown in Figure 8(a), the aluminide coating produced at the $HfCl_4/AlCl_3$ ratio of 1.88 exhibited a high aspect ratio (average grain diameter to coating thickness) of ~3 to 5. This coating was about 3 times thicker than the coating formed on the Ni alloy for the same aluminizing time (Figures 3 and 8).

The surface of all the coating specimens formed on pure Ni was significantly distorted and damaged. In many parts of the coatings, cracks were observed between columnar grains (Figure 8(a)), and some grains were delaminated from the substrate (Figure 8(b)). The XRD analysis was difficult because of the damaged surface of the coating specimens. Nevertheless, normal θ-2θ XRD results indicated that β, γ', γ'_M (a martensitic phase of γ'), and Hf_2Ni_7 phases coexisted in the coating layer with some unidentified small peaks. It

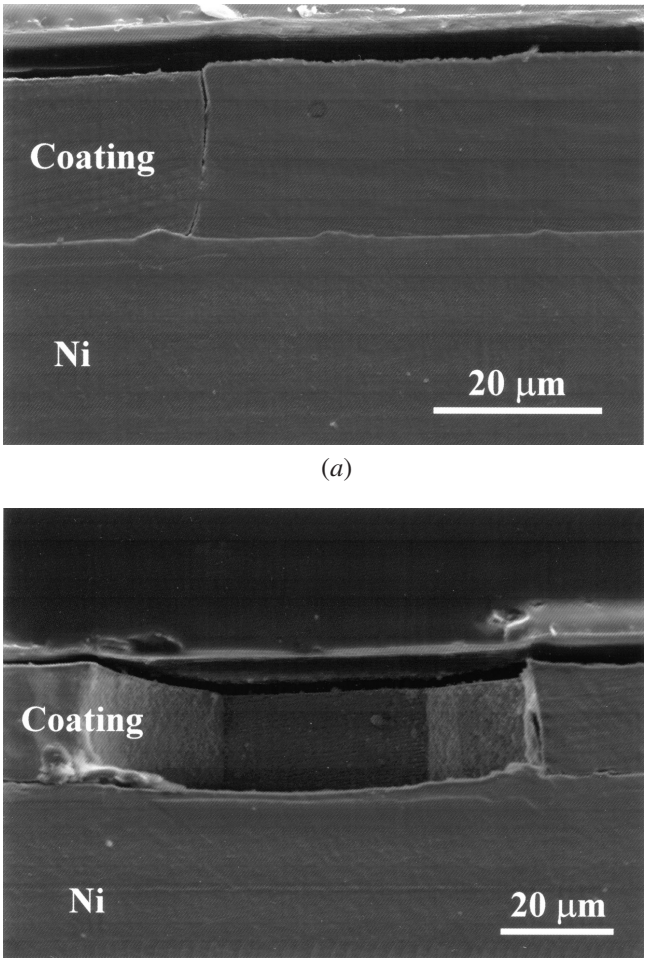

Fig. 8—(a) and (b) SEM cross-section images of the aluminide coating formed on pure Ni at the $HfCl_4/AlCl_3$ ratio of 1.88.

appeared that the damage occurred due to a significant volume change when some of the β-NiAl coating matrix formed at 1150 °C underwent a martensitic phase transformation (β to γ'_M) during rapid sample cooling.

Figure 9 shows the compositional profiles of the aluminide coating produced at the $HfCl_4/AlCl_3$ ratios of 0.75 and 1.88. Based on our experience with the coating specimens formed on the Ni-alloy substrates, we were able to obtain the compositional profiles at the very top of the coating surface by (1) shortening the time used to calibrate and stabilize the GDMS instrument, (2) using a lower sputtering rate (~0.1 μm/min), (3) setting the equipment to detect Hf before measuring Ni and Al, and (4) reducing the number of elements (*i.e.*, only Ni, Al, and Hf) measured. Note that the GDMS instrument is usually set up to measure one element at a time, from the lightest to the heaviest.

For the coating produced at the $HfCl_4/AlCl_3$ ratio of 0.75 (Figure 9(a)), the Ni and Al concentration profiles were relatively constant at ~81.6 and ~17.7 wt pct, respectively, in the coating layer. The Hf concentration was the highest in the middle of the coating matrix at ~0.03 wt pct and decreased sharply at the coating surface, as well as at what appeared to be the diffusion region between the coating and the substrate. However, some minor segregation of Hf and

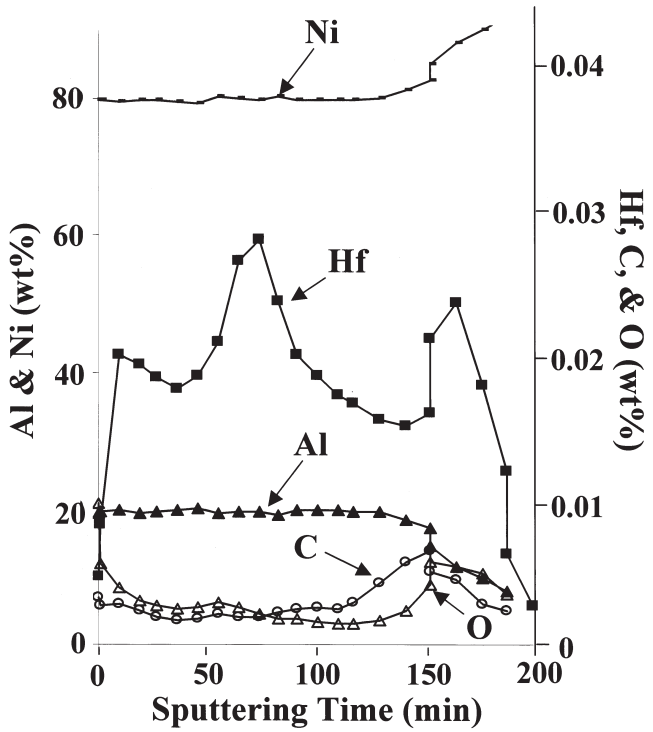

(*a*)

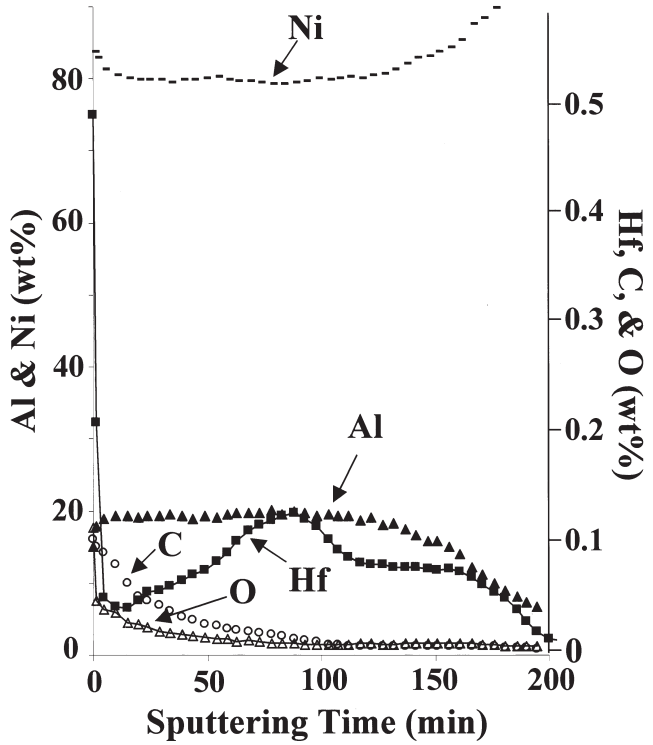

(*b*)

Fig. 9—GDMS profiles through the aluminide coating specimens formed on pure Ni at the $HfCl_4/AlCl_3$ ratio of (*a*) 0.75 and (*b*) 1.88.

minor impurities (~0.05 wt pct O and C) were observed at this ratio. Similarly, the coating produced at the $HfCl_4/AlCl_3$ ratio of 0.19 also contained about ~0.02 to 0.03 wt pct Hf in the middle of the coating layer (the data are not shown).

Figure 9(b) is the Hf concentration profile for the aluminide coating produced at the $HfCl_4/AlCl_3$ ratio of 1.88. The Ni and Al concentration profiles were uniform (~79.7 wt pct Ni and ~19.4 wt pct Al), which corresponded to ~65.4 at. pct Ni and ~34.6 at. pct Al, respectively. The Hf concentration ranged from ~0.05 to 0.12 wt pct through the coating thickness. The Hf concentration increased up to ~0.5 wt pct at the coating surface, which was ~4 times higher than that measured at the middle of the coating matrix. At the same time, the Ni concentration increased to ~83.8 wt pct (~71.7 at. pct), while Al decreased to ~15.1 wt pct (~28.1 at. pct) at the surface. Furthermore, the segregation of O and C (~0.1 wt pct) was observed at the coating surface along with the Hf segregation.

For all the coating samples produced on pure Ni, the average Ni concentration in the coating matrix was in the range of ~65.4 to 67.9 at. pct, and that of Al was between ~32.1 and ~34.6 at. pct. Note that the relative Ni and Al concentrations were similar to those measured for the aluminide coating formed on the Ni alloy (~64 at. pct Ni and ~34 at. pct Al). In accordance with the Ni-Al binary-phase diagram at 1150 °C, β-NiAl as the major phase and γ'-Ni_3Al as a minor phase (~10 pct) are expected to be stable at this composition range.

However, at the coating surface, the Ni and Al concentrations of the aluminide coating formed at the $HfCl_4/AlCl_3$ ratio of 1.88 were ~83.8 wt pct (71.7 at. pct) Ni and ~15.1 wt pct (28.1 at. pct) Al (Figures 8(a) and (b)), respectively. This Ni/Al atomic ratio of 2.6 was closer to the composition of γ'-Ni_3Al than to that of β-NiAl. On the other hand, the Ni and Al concentrations measured at the coating surface for the lower $HfCl_4/AlCl_3$ ratios were ~65.3 and ~34.7 at. pct, respectively. These results suggested that the coating surface was γ'-Ni_3Al at the higher $HfCl_4/AlCl_3$ ratio, which coincided with the Hf segregation at the coating surface. However, the presence of γ'-Ni_3Al could not be confirmed by grazing incidence x-ray diffraction (GIXRD), due to the surface distortion of the coating specimens, as mentioned earlier.

IV. DISCUSSION

A. *Key Observations from the Present Work*

The coating specimens produced on the Ni alloy by the continuous doping procedure as well as by the pure aluminizing procedures exhibited a similar columnar microstructure. As shown in Figure 3, the coating microstructure consisted of a β-NiAl coating matrix and a thin layer of γ'-Ni_3Al at the surface of the coating matrix. The only major difference was the amount of the γ'-Ni_3Al phase present at the coating surface, which substantially increased with Hf incorporation (Figure 4). Another key observation was the low amount of Hf incorporated into the coating matrix from the gas phase. For example, the average Hf/Al atomic ratio in the coating layer was only ~0.005 at the highest $HfCl_4/AlCl_3$ partial-pressure ratio of 0.67 used in this study. In this section, we attempt to explain these observations by considering thermodynamics and the diffusion behavior in γ'-Ni_3Al and β-NiAl, while comparing the present results with our prior observations from pure aluminizing.

B. *Prior Observations on Formation of the γ'-Ni_3Al Layer at the Coating Surface*

Before our experimental observations can be discussed in a meaningful manner, we need to understand the growth behavior of the nondoped aluminide coating shown in Figure 3(a). In our prior work,[23] the existence of the γ'-Ni_3Al layer at the coating surface was observed, as the Ni alloy surface was aluminized (without Hf doping) as a function of time in the range of 5 to 180 minutes. After 5 minutes of aluminizing, the alloy surface consisted of ~100-nm-sized γ'-Ni_3Al particles randomly nucleated, with significant amounts of heavy alloying elements (Ta and W) segregated to the coating surface and to grain boundaries. Within 20 minutes, the coating matrix grew vertically as well as laterally to contain preferentially oriented columnar β-NiAl grains with aspect ratios of 3 to 5. The γ'-Ni_3Al layer was detected at the coating surface along with the segregation of Ta and W, even after 20 minutes of aluminizing. With further increases in the aluminizing time, the γ'-Ni_3Al layer at the coating surface did not disappear. The thickness of the γ'-Ni_3Al layer was ~200 to 300 nm and did not change with increasing aluminizing time.

These observations indicated that (1) the γ'-Ni_3Al layer formed first, before the β-NiAl phase formed on the Ni alloy surface, and (2) the β-NiAl coating matrix grew underneath this apparently "floating" γ'-Ni_3Al layer during aluminizing. In our prior work, we speculated that these phenomena could be attributed to the continued segregation of Ta and W at the coating surface, due to the transport of these elements through grain boundaries from the substrate to the coating surface. These phenomena could be further explained from a thermodynamic point of view.

C. *Review of the Effective Heat of Formation Model*

Recently, the effective-heat-of-formation (EHF) model was been developed to predict the sequence of phase formations in thin-film binary metal-metal systems.[29] The success of the EHF model comes from considering the concentration of the reactants at the growth interface. In order to comprehend this model, the concept of an EHF ($\Delta H'$) must be defined.[29]

$$\Delta H' = \Delta H^\circ \times \frac{x'}{x} \qquad [1]$$

where ΔH° is the standard heat of formation (kJ/mol.atom) at 298 K, x' is the effective concentration of an element between two reacting elements at the growth interface, and x is the concentration of the element in the compound after the reaction is completed at the interface. In Figure 10(a), the EHF values are plotted as a function of effective concentration for the Ni-Al system.[29] Each triangle represents the energy ($\Delta H'$) released as a function of the effective concentration during the formation of a particular Ni-Al phase.[29]

For example, consider annealing of a thin Al film deposited on a Ni substrate. It has been a well accepted fact in solid-state diffusion that the lower the melting point, the greater the atomic mobility.[29,30] Thus, the most rapid mixing is expected to take place at the composition of the liquidus minimum (the lowest eutectic temperature) in the binary system. This liquidus composition corresponds to the effective

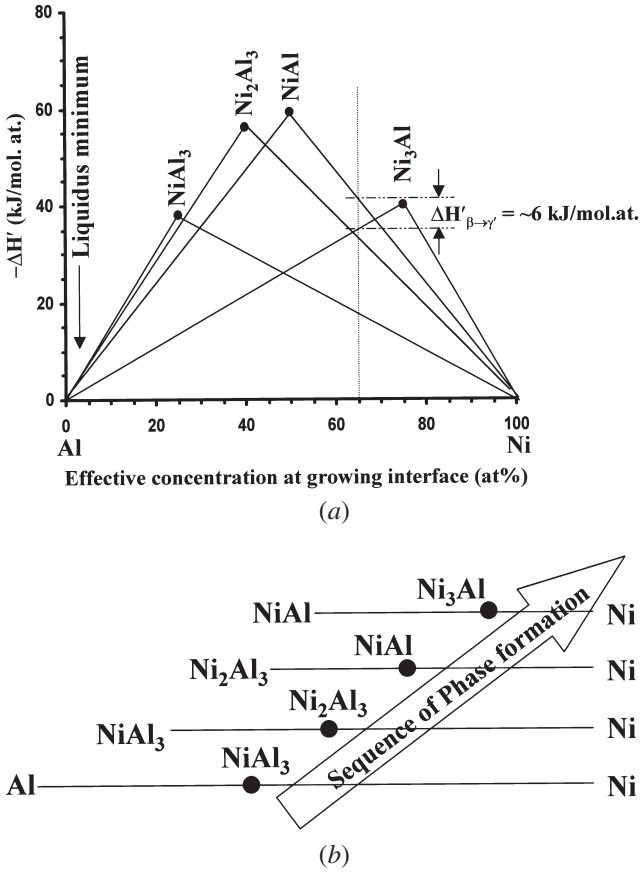

Fig. 10—The EHF diagram previously constructed for the NiAl system by Pretorius *et al.*[29] The effective concentration at the β-NiAl side of the interface between the γ'-Ni_3Al and β-NiAl layers was estimated from the GDMS profiles shown in Fig. 9(b). (*b*) The sequence of phase formation for a thin film of Al deposited on a pure Ni substrate predicted by the EHF model and experimentally observed.[30,34]

concentration at the growing side of the Al/Ni interface.[29] In the Ni-Al system, the liquidus minimum is located between the Ni and $NiAl_3$ phases, as marked in the EHF diagram (Figure 10(a)). At this effective concentration, the formation of $NiAl_3$ results in the greatest release of heat. Therefore, $NiAl_3$ is the first phase to form before any other phases in the Ni-Al system. After all of the Al thin film is consumed by the formation and growth of the $NiAl_3$ phase, the effective concentration moves in the direction of the Ni-rich region. Then, the next phase to form is Ni_2Al_3 at the expense of $NiAl_3$. This sequence will be followed by NiAl and Ni_3Al, as illustrated in Figure 10(b).[29,31]

In this model, the standard heat of formation (ΔH°) at 298 K is mainly considered, since ΔH° is a good measure of the Gibbs free energy (ΔG°), especially for binary systems where compounds have large negative ΔH° values. Since the heat capacity of products is approximately equal to that of the reactants ($\Delta C_p \approx 0$) for reactions occurring in the solid state (the Neumann–Kopp rule),[32] the temperature dependence of ΔH° and ΔS° is usually negligible. As listed in Table III, the values of ΔH° and ΔS° calculated for the Ni-Al system at 298 and 1373 K using the HSC Chemistry Thermodynamic Program[33] show that these quantities are not significantly dependent on temperature. Also, entropy contributions to the change in the Gibbs free energy of

Table III. ΔH_T and ΔS_T Estimated for Intermetallic Compounds in the Ni-Al System

$\Delta H°_T$					
	at 298 K		at 1373 K		
Compounds	kJ/mol	kJ/mol·at.	kJ/mol	kJ/mol·at	
Ni_3Al	−153	−38	−175	−44	
NiAl	−118	−59	−138	−69	
Ni_2Al_3	−282	−56	−335	−67	
$NiAl_3$	−150	−37	−192	−48	
$\Delta S°_T$					
	at 298 K		at 1373 K		
Compounds	J/K·mol	J/K·mol·at.	J/K·mol	J/K·mol·at	$T\Delta S°_{(1373\ K)}$ kJ/mol·at
Ni_3Al	−4	−1	−32	−8	−11
NiAl	−4	−2	−28	−14	−19
Ni_2Al_3	−8	−2	−71	−14	−19
$NiAl_3$	−4	−1	−51	−13	−18

formation (*i.e.,* $T\Delta S°$) are smaller than the enthalpy contributions previously studied.[34,35]

The EHF model has been experimentally validated by other research groups for various binary systems.[31,36,37] For example, Colgan[31] showed that as both annealing time and temperature increased, an Al thin film on a Ni substrate (prepared by PVD) followed exactly the sequence of phase formations predicted by the EHF model. Also, for aluminizing a pure Ni substrate at high-Al-activity and low-temperature conditions (870 °C, as opposed to the value of 1150 °C used in this investigation), Hickl and Heckel[36] observed that Ni_2Al_3 was the first layer to form (since $NiAl_3$ is a liquid at 870 °C), followed by the formation of a thinner layer of NiAl and an even thinner layer of Ni_3Al between the $NiAl_3$ layer and the Ni substrate. Upon subsequent annealing at 1000 °C, the NiAl layer grew at the expense of the Ni_2Al_3 layer, while the Ni_3Al layer remained relatively unchanged for the duration of the annealing.

D. *Effects of "γ′ Formers"*

As mentioned earlier, our experimental observations suggested that, whether the coating was doped with Hf or not, (1) the γ'-Ni_3Al layer formed first at the alloy surface and (2) the formation and growth of the β-NiAl coating matrix followed, while the γ'-Ni_3Al layer continued to remain at the surface of the growing coating layer. At first glance, the observed sequence was not in agreement with that predicted by the EHF model. However, it is critical to recognize that the sequence of phase formation can be changed by other factors such as stress/strain, diffusion barriers, and impurities, if those factors change the free energy of the coating system.[29] For example, an elastic-enthalpy change caused by a lattice-parameter difference between the coating and substrate can result in an alteration of the phase-formation sequence.

It is well known that the solubility of Hf, Mo, Ta, Ti, and W in Ni alloys increases in the following phase order: β-NiAl, γ-Ni, and γ'-Ni_3Al.[38,39] Therefore, these elements are commonly referred to as γ' formers. For example, at 1100 °C, the equilibrium ratio of Ta between γ' and β (*i.e.,* $K^{\gamma'/\beta}$) is 2.29, and $K^{\gamma'/\beta}$ for W is 8.67. It appears that $K^{\gamma'/\beta}$ for Hf has not been measured (or reported) yet. The γ' formers are larger than Ni and Al. Bozzolo *et al.*[39] showed that there is a linear relationship between the concentration of a γ' former in β-NiAl and its lattice parameter. This behavior appears to be the cause of low solubility limits of the γ' formers in β-NiAl. Al lattice sites in γ'-Ni_3Al have more space to accept the larger impurities with less strain-energy accumulation, since γ'-Ni_3Al has both a slightly larger unit-cell-volume to atomic-volume ratio than that of β-NiAl and a larger Al radius due to an increased Al coordination number over that of β-NiAl. When γ' formers are present as impurities and certain concentration levels are reached, the elements may cause a significant elastic-enthalpy change of β-NiAl through lattice distortion. Then, under these situations, the γ'-Ni_3Al can become energetically more stable than the β-NiAl phase.

The formation of the γ'-Ni_3Al phase observed before the β-NiAl phase in our coating surface can be attributed to the incorporation of Ta and W from the substrate at the initial stage of aluminizing, in the case of Ni-alloy substrates. The Hf doping procedure enhanced the amount (or thickness) of the γ'-Ni_3Al layer during the coating growth. On the other hand, the role of the Hf doping on the formation of the γ'-Ni_3Al layer appeared to be more profound for the coating specimens produced on pure-Ni substrates, as shown in Figure 9. For these coating specimens, Hf from the gas phase, *via* the decomposition of $HfCl_4$, was the only source of γ'-forming elements. The external coating layer of these samples exhibited the average Ni and Al contents (~80 and ~20 wt pct, respectively). These values were equivalent to ~65 and ~35 at. pct, which corresponded to a Ni-rich hypostoichiometric β-NiAl composition. For the sample doped at the low $HfCl_4/AlCl_3$ ratio (Figure 9(a)), the compositions at the coating surface were not different. In these samples, no Hf segregation and no compositional changes in Al or Ni were observed at the coating surface (Figure 9(a)). In comparison, for the sample doped at the higher $HfCl_4/AlCl_3$ ratio (Figure 9(b)), the Hf concentration increased from ~0.12 wt pct (~0.03 at. pct) to 0.5 wt pct (~0.14 at. pct) at the coating surface. Meanwhile, the Ni concentration increased to ~84 wt pct (~72 at. pct) and the Al concentration decreased to ~15 wt pct (28 at. pct), which were closer to the Al-rich γ'-Ni_3Al phase composition. These results suggested that, when the Hf concentration reached a certain level in the β-NiAl coating layer, Hf atoms were rejected to the coating surface from the β-NiAl coating matrix and caused the formation of the γ' phase.

The elastic-enthalpy change in β-NiAl caused by adding ~0.14 at. pct Hf (the GDMS value shown in Figure 9(b)) was calculated to be ~+6.3 kJ/mol using the method previously developed by Blum and Hess:[40]

$$\Delta H' = \frac{1}{2} k \left(\frac{\Delta V}{V} \right)^2 \qquad [2]$$

This value was similar to the $\Delta H'$ difference (~+6 kJ/mol) between β-NiAl and γ'-Ni_3Al at the effective Ni composition of 65 at. pct shown by the EHF diagram in Figure 10(a). This comparison indicated that ~0.14 at. pct Hf could be sufficient to make γ'-Ni_3Al more stable than β-NiAl due to the increase in the elastic enthalpy of the β-NiAl phase.

E. *Why Does the γ′-Ni_3Al Layer Remain at the Coating Surface?*

As described earlier, once the β-NiAl phase formed, the overall growth of the aluminide coating was mainly associated with the expansion of the β-NiAl layer, whereas the thickness of the γ′-Ni_3Al layer at the coating surface did not significantly change with up to 180 minutes of aluminizing time.[23] These observations suggested that the γ′-Ni_3Al phase apparently "floated" at the coating surface during aluminizing in Figure 11. These observations also implied that the growth of the β-NiAl layer occurred at the γ′-Ni_3Al/β-NiAl interface. If not, the γ′-Ni_3Al phase should have been imbedded in the β-NiAl coating matrix. However, in order for this floating phenomenon to occur, the following conditions must be met: (1) the diffusion of Al had to be relatively faster than that of Ni through the γ′-Ni_3Al layer, and (2) the diffusion of Ni had to be faster than that of Al through the β-NiAl layer.

The diffusion in β-NiAl and γ′-Ni_3Al is strongly influenced by defect chemistry. Ikeda *et al.*[41] reported that the interdiffusion coefficient of γ′-Ni_3Al was $\sim 7 \times 10^{-9}$ cm^2/s at 26 at. pct Al and $\sim 4 \times 10^{-9}$ cm^2/s at 24 at. pct Al. They also reported that the diffusion of Al was slower than that of Ni in γ′-Ni_3Al at the stoichiometric composition. However, the diffusion of Al appeared to be equivalent to or higher than that of Ni at 26 at. pct Al, as summarized in Table IV. This behavior was attributed to the crystal structure of γ′-Ni_3Al ($L1_2$). In this structure, a Ni atom is the nearest neighbor to eight Ni atoms as well as four Al atoms, while an Al atom is surrounded only by Ni atoms.[35] Thus, a Ni atom can exchange its position with its nearest Ni site without producing disorder in the $L1_2$ structure, but an Al atom must exchange its position only with the nearest Ni atom, to preserve the $L1_2$ structure. In Al-rich γ′-Ni_3Al, however, the diffusion of Al can proceed by antistructure defects on the Ni sublattice (*i.e.,* vacancies created in the Ni sites due to extra Al on the Ni sublattice); thus, the movement of Al atoms can be drastically enhanced. As shown in Figure 9(b), the average Al concentration measured at the coating surface in our study was ~15.1 wt. pct (~28 at. pct), which corresponded to an Al-rich γ′-Ni_3Al composition. Comparison of our observations with the results reported by Ikeda *et al.* suggested that the inward diffusion of Al could certainly be faster than the outward diffusion of Ni through the Al-rich γ′-Ni_3Al layer.

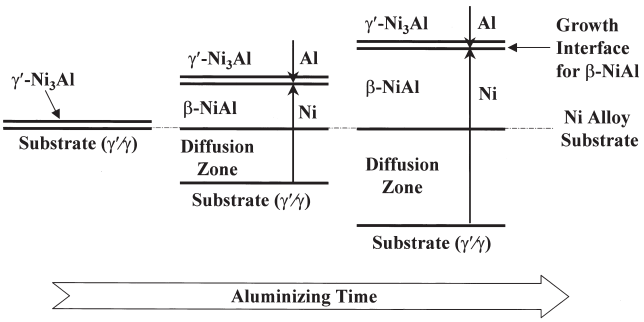

Fig. 11—Schematic representation of the floating behavior of the γ′-Ni_3Al layer at the coating surface.

Shanker and Seigle[42] reported that the interdiffusion coefficient measured from a Ni-rich β-NiAl coating grown on a pure-Ni substrate at 1100 °C was $\sim 3 \times 10^{-9}$ cm^2/s. Based on internal marker movement and Matano interface analysis, they determined that Ni diffusion was ~3 times faster than that of Al, as summarized in Table IV. Therefore, the parabolic kinetics observed for the growth of the Ni-rich β-NiAl layer was attributed to the outward diffusion of Ni from the Ni substrate to the coating surface, where Ni reacted with $AlCl_3$ in the presence of H_2. This interpretation has been consistent with observations made by other investigators.[42,43,44]

In addition to these diffusivity considerations, the floating phenomenon requires another explanation about the driving force for the inward diffusion of Al through the γ′-Ni_3Al layer. It appeared that, during aluminizing, a negative Al concentration gradient could have been established through the thickness of the γ′-Ni_3Al layer by (1) the depletion of Al at the γ′-Ni_3Al/β-NiAl interface and (2) the generation of Al at the gas/γ′-Ni_3Al interface by the decomposition of $AlCl_3$ in H_2. If this was true, the Al concentration at the coating surface should have been higher than that at the γ′-Ni_3Al/β-NiAl interface. However, we were not able to measure this concentration gradient in the present study, to confirm this interpretation.

F. *High $HfCl_4$ Concentration Required for Hf Doping*

Figure 9(a) shows that the average Hf concentration in the β-NiAl coating matrix formed on pure Ni without γ′-Ni_3Al formation at the coating surface was ~0.02 wt pct (~0.005 at. pct). On the other hand, with the formation of γ′-Ni_3Al at the coating surface, the Hf concentration was ~0.12 wt pct (~0.03 at. pct), as shown in Figure 9(b). The existence of the γ′-Ni_3Al/β-NiAl interface suggested that the β-NiAl coating matrix was most likely saturated by Hf during the second sequence of the continuous doping procedure. In other words, the Hf concentration (~0.12 wt pct, or ~0.03 at. pct) could most likely be the solubility limit of Hf in the Ni-rich β-NiAl coating layer.

Our literature research to date indicated that Hf solubility limits in β-NiAl and γ′-Ni_3Al have not been explicitly measured or reported in the open literature. Also, observations on Hf-rich precipitate formation in the β-NiAl matrix appeared to be substantially different from one group to the other, based on sample preparation (*e.g.,* casting or coating), the stoichiometric composition of NiAl, as well as alloyed impurities.[10,45] For example, Locci *et al.*[45] observed, using a TEM, that the precipitation of the Heusler phase (Ni_2AlHf) in single-crystal cast β-NiAl contained

Table IV. Comparison of Ni and Al Diffusion Coefficients in β-NiAl and γ′-Ni_3Al Phases at 1100 °C

Interdiffusion coefficient	Ni-rich (~64 at. pct) β-NiAl Phase*	Al-Rich (~26 at. pct) γ′-Ni_3Al Phase**
	$\sim 3 \times 10^{-9}$	$\sim 7 \times 10^{-9}$
D_{Ni} (cm^2/s)	$\sim 5.7 \times 10^{-9}$	$\sim 6.7 \times 10^{-9}$
D_{Al} (cm^2/s)	$\sim 1.8 \times 10^{-9}$	$\sim 7.8 \times 10^{-9}$

*Ref. 45.
**Ref. 42.

~0.49 wt pct Hf and 0.17 wt pct Si along with $Ni_{16}Hf_6Si_7$ (*G*-phase) formation. But, they have not examined the lower Hf-concentration range. Note that the presence of Si is known to enhance the formation of *G*-phase precipitates.[45] Based on oxidation studies of polycrystalline cast Hf-doped stoichiometric β-NiAl, the Hf solubility limit has been suggested to be ~0.2 wt pct (0.05 at. pct),[9] which was in agreement with the concentration measured in this study of ~0.12 wt pct (~0.03 at. pct).

In accordance with the EHF model, Hf incorporation into the β-NiAl coating matrix increases the elastic enthalpy of the β-NiAl phase due to the large size of Hf. Thus, the Hf incorporation became increasingly thermodynamically unfavorable with increasing Hf content. Once its solubility limit was reached, it resulted in the formation of the γ'-Ni_3Al layer at the coating surface, as clearly shown in Figure 9, for pure-Ni substrates. Once the γ'-Ni_3Al layer was formed, the Hf incorporation into the β-NiAl layer is dictated by the partitioning of Hf at the γ'-Ni_3Al/β-NiAl interface, based on the difference in apparent Hf solubility in these two phases.

The Hf incorporation behavior observed for the Ni-alloy substrate was much more complex and difficult to interpret than that for pure Ni. As discussed in the previous section, at low $HfCl_4$ concentrations, it appeared that the source of Hf incorporated into the coating matrix formed on the Ni-alloy substrate (Figure 7) was primarily the alloy itself ("autodoped"), instead of $HfCl_4$ in the gas phase, as Hf and the other refractory elements partitioned into the β-NiAl layer from the alloy. For example, similarities in the Ta and Hf profiles, particularly at the coating-substrate region, indicated that Hf incorporated into the coating layer was mainly from the substrate. Therefore, the β-NiAl coating layer appeared to be already saturated with the refractory elements. Evidence for this interpretation was the presence of the γ'-Ni_3Al layer at the coating surface, whether the coating was doped or not. In this regard, the higher Hf concentration measured at high $HfCl_4/AlCl_3$ concentrations (Figure 7) should be interpreted as a result of formation of Hf-rich precipitates, mainly at grain boundaries of the coating matrix. Figure 3 shows evidence for the segregation of bright-contrast particles at grain boundaries. These particles are suspected to be Hf-rich precipitates, although their compositions could not be directly confirmed by the spatial- and composition-resolution limitations of the EMPA technique.

V. CONCLUSIONS

The coating specimens produced on the Ni alloy by the continuous doping procedure, as well as the pure aluminizing procedures, exhibited a similar columnar microstructure. With the continuous doping procedure, the amount of the thin γ'-Ni_3Al layer present at the β-NiAl coating surface substantially increased. In accordance with the EHF model, the formation of the γ'-Ni_3Al phase at the coating surface was attributed to an increase in the elastic enthalpy of the β-NiAl phase associated with the segregation of refractory alloying elements, in the case of pure aluminizing. It appeared that, during the continuous doping procedure, the formation of the γ'-Ni_3Al phase increased with the additional segregation of Hf. The results also suggested that the growth of the β-NiAl layer mainly occurred at the γ'-Ni_3Al/β-NiAl interface, which apparently made the γ'-Ni_3Al layer "float" at the coating surface during the aluminizing process.

Another key observation from the continuous doping experiments was that the amount of Hf incorporation from the gas phase into the coating matrix was extremely low. Rather high $HfCl_4$ concentrations were needed to incorporate Hf into the β-NiAl matrix. In the case of pure Ni substrates, it appeared that the Hf incorporation became increasingly thermodynamically unfavorable with increasing Hf content in the β-NiAl layer. Once its solubility limit was reached (~0.12 wt pct, or ~0.03 at. pct), the formation of the γ'-Ni_3Al layer at the gas/solid surface was observed with the segregation of Hf up to ~0.5 wt pct, as detected by GDMS. After the γ'-Ni_3Al layer was formed, the incorporation of Hf into the β-NiAl layer was most likely dictated by the difference in apparent Hf solubility between the γ'-Ni_3Al and β-NiAl layers.

The incorporation mechanism of Hf into the aluminide coating formed on the Ni alloy was apparently different from those observed for the pure-Ni substrates due to the presence of other refractory elements in the alloy. The Hf content measured in the β-NiAl layer (~0.01 wt pct) was very low at the low $HfCl_4/AlCl_3$ ratios. Similarities in the Ta and Hf profiles, particularly at the coating-substrate region, indicated that Hf incorporated into the coating layer was mainly from the substrate. Therefore, at the low $HfCl_4/AlCl_3$ ratios, Hf did not incorporate as a dopant into the growing coating layer from the gas phase, since available Hf substitution sites in the growing β-NiAl coating layer (*via* the γ'-Ni_3Al surface layer) were occupied with the major alloying elements such as Ta partitioned from the Ni alloy substrate. At high $HfCl_4/AlCl_3$ ratios (>~0.6), the precipitation of ~0.1 μm particles (presumably Hf-rich) was observed along grain boundaries of the coating layer, with the overall Hf concentration of ~0.05 to 0.25 wt pct measured for the coating layer by GDMS.

ACKNOWLEDGMENTS

This research was sponsored by the National Science Foundation (Grant No. DMR9801042) and the Advanced Gas Turbine System Program, DOE Office of Industrial Technologies, under Contract No. DE-AC05-96OR22464 with Lockheed Martin Energy Research Corporation, and the Robert C. Stanley Fellowship at Stevens. We thank Dr. Ram Darolia, GEAE, who provided an industrial perspective on our research objectives and progress. We acknowledge contributions to this work by K. Putyera of Shiva Technologies (Syracuse, NY).

REFERENCES

1. G.W. Goward: *Mater. Sci. Technol.*, 1986, vol. 2, pp. 194-200.
2. B. Nagaraj: U.S. Patent 5,427,866, 1995.
3. S.M. Meier, D.M. Nissley, K.D. Sheffler, and T.A. Cruse: *Trans. ASME*, 1992, vol. 114, pp. 258-63.
4. S.M. Meier, D.K. Gupta, and K.D. Sheffler: *J. Met.*, 1991, Mar., pp. 50-53.
5. A. Maricocchi, A. Bartz, and D.J. Wortman: *Proc. 1995 Thermal Barrier Coating Workshop*, W.J. Brindley, ed., NASA Conference Publication No. 3312, Washington, DC, 1995, p. 79.
6. A.W. Funkenbusch, J.G. Smeggil, and N.S. Bornstein: *Metall. Trans. A*, 1985, vol. 16A, pp. 1164-66.
7. D.K. Gupta: U.S. Patent 4,933,329, 1990.

8. B.A. Pint: *Oxid. Met.*, 1996, vol. 45, p. 1.
9. B.A. Pint, I.G. Wright, W.Y. Lee, Y. Zhang, K. Prüβner, and K.B. Alexander: *Mater. Sci. Eng.*, 1998, vol. A245, pp. 201-11.
10. R. Bianco and R.A. Rapp: *J. Electrochem. Soc.*, 1993, vol. 140, pp. 1181-90.
11. R. Bianco and R.A. Rapp: *J. Electrochem. Soc.*, 1993, vol. 140, pp. 1191-203.
12. A. Strawbridge and P.Y. Hou: *Mater. High Temp.*, 1994, vol. 12, pp. 177-81.
13. R. Prescott, D.F. Mitchell, M.J. Graham, and J. Doychak: *Corr. Sci.*, 1995, vol. 37, pp. 1341-64.
14. D.C. Tu, C.C. Lin, S.J. Liao, and J.C. Chou: *J. Vac. Sci. Technol.*, 1986, vol. A4, pp. 2601-06.
15. K.Y. Kim, S.H. Kim, K.W. Kwon, and I.H. Kim: *Oxid. Met.*, 1994, vol. 41, pp. 179-201.
16. K.Y. Kim, J.H. Jun, and H.G. Jun: *Oxid. Met.*, 1993, vol. 40, pp. 321-35.
17. G.W. Goward: presented at the *Metallic Coatings Specialty Workshop*, Hoboken, NJ, Apr. 16, 1997.
18. B.A. Pint and L.W. Hobbs: *J. Electrochem. Soc.*, 1994, vol. 141, pp. 2443-53.
19. J. Stringer, I.M. Allam, and D.P. Whittle: *Thin Solid Films*, 1977, vol. 45, pp. 377-84.
20. Y. Zhang, W.Y. Lee, J.A. Haynes, I.G. Wright, B.A. Pint, K.M. Cooley, and P.K. Liaw: *Metall. Mater. Trans. A*, 1999, vol. 30A, pp. 2679-87.
21. W.Y. Lee, Y. Zhang, I.G. Wright, B.A. Pint, and P.K. Liaw: *Metall. Trans. A*, 1998, vol. 29A, pp. 833-41.
22. W.Y. Lee and G.Y. Kim: *Min. Met. Mater. Soc.*, 1999, pp. 149-60.
23. G.Y. Kim, W.Y. Lee, J.A. Haynes, and T.R. Watkins: *Metall. Mater. Trans. A*, unpublished research, 2003.
24. S.J. Klepeis, J.P. Benedict, and R.M. Anderson: *Mater. Res. Soc. Proc.*, 1988, vol. 115, p. 179.
25. A.P. Mykytiuk, P. Semeniuk, and S. Berman: *Spectrochimica Acta Rev.*, 1990, vol. 13, pp. 1-10.
26. F. Adams and A. Vertes: *Fresenius J. Anal. Chem*, 1990, vol. 337, p. 638.
27. R. Pichoir: in *Materials and Coatings to Resist High Temperature Corrosion*, D.R. Holmes and A. Rahmel, eds., Applied Science Publishers Ltd., London, 1978, pp. 271-91.
28. G.Y. Kim, L.M. He, J.D. Meyer, and W.Y. Lee: *Min. Met. Mater. Soc.*, 2000, pp. 69-78.
29. R. Pretorius, C.C. Theron, A. Vantomme, and J.W. Mayer: *Crit. Rev. Solid State Mater. Sci.*, 1999, vol. 24 (I), pp. 1-62.
30. A.M. Brown and M.F. Ashby: *Acta Metall.*, 1980, vol. 28, pp. 1085-101.
31. E.G. Colgan: *Mater. Sci. Rep.,* 1990, vol. 5, pp. 1-44.
32. O. Kubaschewski and C.B. Alock: *Metallurgical Thermochemistry*, Pergamon Press, Oxford, UK, 1979, p. 184.
33. *HSC Chemistry*, Ver. 4.0, Outokumpu, Poli., Finland.
34. R.D. Noebe, R.R. Bowman, and M.V. Nathal: *Int. Mater. Rev.*, 1993, vol. 38, pp. 193-232.
35. S.V. Divinski, S. Frank, U. Södervall, and C. Herzig: *Acta Mater.*, 1998, vol. 46, pp. 4369-80.
36. A.J. Hickl and R.W. Heckel: *Metal. Trans. A*, 1975, vol. 6, pp. 431-40.
37. G. Ottaviani: *Thin Solid Films*, 1982, vol. 93, p. 127.
38. C.C. Jia, K. Ishida, and T. Nishizawa: *Metall. Mater. Trans. A*, 1994, vol. 25A, pp. 473-85.
39. G. Bozzolo, R.D. Noebe, and F. Honecy: *Min. Met. Mater. Soc.*, 1998, pp. 341-68.
40. W. Blum and D. Hess: *Solid State Ionics*, 1997, vol. 95, p. 41.
41. T. Ikeda, A. Almazouzi, H. Numakura, M. Koiwa, W. Sprengel, and H. Nakajima: *Acta Mater.*, 1998, vol. 46, pp. 5369-76.
42. S. Shankar and L.L. Seigle: *Metall. Trans. A*, 1978, vol. 9A, pp. 1467-76.
43. R. Sivakumar and L.L. Seigle: *Metall. Trans. A*, 1976, vol. 7A, pp. 1073-79.
44. L. Singheiser and G. Wahl: *Thin Solid Films*, 1983, vol. 107, pp. 443-54.
45. I.E. Locci, R.M. Dickerson, A. Garg, R.D. Noebe, J.D. Whittenberger, M.V. Nathal, and R. Darolia: *J. Mater. Res.*, 1996, vol. 11, pp. 3024-38.